Ocean Sci. J. (2012) 47(3):331-345
http://dx.doi.org/10.1007/s12601-012-0032-4

Article

Available online at www.springerlink.com

SpringerLink

Ocean Science Journal

Variability of Suspended Particulate Matter in the Bohai Sea from the Geostationary Ocean Color Imager (GOCI)

Kevin Ruddick[1]*, Quinten Vanhellemont[1], Jing Yan[2], Griet Neukermans[1,3,4], Guomei Wei[2], and Shaoling Shang[2]

[1]*Management Unit of the North Sea Mathematical Models (MUMM), Royal Belgian Institute for Natural Sciences (RBINS), 100 Gulledelle, 1200 Brussels, Belgium*
[2]*Research and Development Center for Ocean Observation Technologies, Xiamen University, Xiamen 361005, China*
[3]*Université du Littoral Côte d'Opale, 62930 Wimereux, France*
[4]*Now at: Marine Physical Laboratory, Scripps Institution of Oceanography, University of California, San Diego, La Jolla, CA 92093, USA*

Received 3 April 2012; Revised 24 June 2012; Accepted 30 August 2012

Abstract – This study assesses the performance of the Geostationary Ocean Imager (GOCI) for mapping of suspended particulate matter in the Bohai Sea, a turbid water region. GOCI imagery for remote sensing reflectance and Total Suspended Solids (TSS) is analysed in detail for two days in June 2011 (8 images per day). Both instantaneous and daily composite maps are considered and a comparison is made with corresponding reflectance and TSS products from MODIS-AQUA. Results show TSS distributions corresponding to previous studies of the region. The advantage of the higher acquisition frequency (8 images/day instead of 1) offered by GOCI is clearly demonstrated in the daily composite which is more complete during this period of scattered but moving clouds. Consideration of temporal variation over the day indicates low natural variability but some artificial variability from processing errors – this analysis provides a first indication of how the higher frequency of data from geostationary ocean colour could lead to improved data quality control via temporal coherency outlier detection. While there is room for improvement on the GOCI calibration, atmospheric correction and retrieval algorithms, the current study suggests that the GOCI data can already be used now to study qualitatively sediment dynamics except in the extremely turbid waters which are masked out of the current dataset. In a wider context, it is considered that the technical challenges of geostationary ocean colour have been met by the GOCI concept, and, notwithstanding potential improvements on the concept and data processing methods, it is recommended that this mission serve as a model for future geostationary ocean colour sensors over Europe/Africa and the Americas.

Key words – geostationary, ocean, GOCI, Bohai Sea, suspended particulate matter

*Corresponding author. E-mail: K.Ruddick@mumm.ac.be

1. Introduction

Until the launch of GOCI, all major ocean colour sensors have been operated from satellite platforms in sun-synchronous near polar orbit, typically 700-800 km from the earth's surface. This orbit provides good global coverage from a single wide-swath sensor, e.g. MODIS-AQUA with swath of 2330 km, gives at least one image per day at latitude 51° with higher frequency of sampling for polar regions and lower frequency (slightly less than daily) for tropical regions. However, once daily imagery is insufficient for many applications in coastal waters, where processes at higher frequency (tidal, diurnal) may need to be resolved. Moreover, in many regions the effective frequency of data is dramatically reduced by clouds, giving periods of days or even weeks without data. The geostationary orbit, in contrast, offers the possibility of frequent sampling during the day, e.g. every 15 minutes or even every 5 minutes for the SEVIRI sensor, a sensor with broad red and near infrared bands which was designed for meteorological applications and operates onboard the METEOSAT Second Generation platforms (Schmetz et al. 2002). This brings important new opportunities (IOCCG 2012; Neukermans 2012):

- The vastly improved frequency of sampling increases the chances of acquiring useful data during periods of scattered clouds, thus reducing a critical obstacle to operational use of ocean colour remote sensing, e.g. for

water quality monitoring or harmful algae bloom detection.
- High frequency processes may be resolved during cloud-free daylight periods, opening up the possibility of studying, from space, processes such as tidal resuspension of bottom sediments, horizontal advection of river plumes, diurnal variation of photosynthetic parameters, vertical migration of plankton, etc.
- The stronger temporal correlation between data from consecutive images, e.g. 1 hour apart instead of 1 day, should improve the potential for quality control of ocean colour data processing algorithms using outlier detection algorithms, e.g. (Sirjacobs et al. 2011).

However, the geostationary orbit also brings new difficulties and challenges. The much higher orbit (35 786 km) requires a larger, and hence heavier and more expensive, telescope to achieve the same spatial resolution as a polar-orbiter. The viewing geometry above the equator also gives higher air mass (atmospheric path length) at higher latitudes, and hence critical problems for atmospheric correction, especially for blue wavelengths. Also, the spatial resolution is lower at higher latitudes, decreasing from the nadir point at the equator. Furthermore, the polar regions are not viewed and airmass increases dramatically for viewing angles above 65°. The geostationary geometry limits sunglint problems to equatorial areas (generally between 10°N and 10°S), with the sunglint spot moving from East to West along with the sun's position (Mazeran and Meskini 2008).

In a study using the SEVIRI sensor, (Neukermans et al. 2009) demonstrated the feasibility of the geostationary ocean colour approach for measuring the tidal variability of suspended sediments in the turbid waters of the southern North Sea (52°N). Despite the coarse spectral and radiometric resolution of the SEVIRI sensor, an atmospheric correction scheme was developed giving suspended matter products that were comparable to those of MODIS-AQUA. In a follow up study (Neukermans et al. 2012b) used SEVIRI to map high frequency variability of correlated parameters such as turbidity and diffuse attenuation of Photosynthetically Available Radiation and validated the remotely sensed data with measurements from optical sensors on moored buoys.

In 2010 the GOCI (Geostationary Ocean Imager) sensor (Faure et al. 2008) was launched onboard the geostationary COMS satellite, thus heralding a new era for ocean colour remote sensing. GOCI has spectral bands similar to those of SeaWiFS, but with an extra red band instead of 510 nm and a near infrared band at 745 nm instead of the 765 nm band which was prone to oxygen absorption. The 8 GOCI bands are centred on 412 nm, 443 nm, 490 nm, 555 nm, 660 nm, 680 nm, 745 nm and 865 nm. The full characteristics of the GOCI sensor and mission are presented in the companion papers to this Special Issue.

This study presents some early data from the GOCI mission, with the objective of assessing data quality, providing recommendations to mitigate any identified shortcomings in the sensor and/or data processing and, more generally, to learn from this first geostationary ocean colour mission. This experience will be particularly valuable for optimising the design of a whole new generation of geostationary ocean colour missions over Europe/Africa, the Americas and Asia – see Appendix A of (IOCCG 2012) for the plans of the respective space agencies.

The specific questions to be addressed in this study, relating to the GOCI mission are:

- Are the GOCI level 2 data for remote sensing reflectance and Total Suspended Solids (TSS, also called SPM or TSM) suitable for investigating variability of suspended particulate matter in the Bohai Sea?
- Are there any weaknesses in the GOCI level 2 data that can be identified and improved in future processing?

The specific questions to be addressed relating to the geostationary ocean colour concept more generally are:

- What advantage can be obtained from geostationary ocean colour as regards data availability in periods of scattered clouds?
- What natural processes can be studied by geostationary ocean colour that cannot be seen by polar-orbiting sensors?
- Can the high frequency of data from geostationary ocean colour be used to improve quality control of data by consideration of temporal coherency?

Obviously the extent to which these questions can be addressed at present depends on the quality of the GOCI sensor and processing.

The Bohai Sea, bordering the coast of North East China, has been chosen as the study area here, because of the existing knowledge of oceanographic processes in this region (Guan 1994; Zhang 1996; Wei et al. 2004), and

because of its suitability as a turbid water region with high tidal variability. Suspended Particulate Matter (SPM) has previously been studied in this region by (Cui et al. 2010) who validated the MERIS SPM product using in situ data. The MERIS SPM product was also used by (Chen et al. 2010) in conjunction with numerical modeling for study of SPM dynamics in this region. Empirical and neural network SPM algorithms were proposed for use with MODIS data in this region by (L Wang et al. 2012) and (Wang and Li 2007) respectively.

2. Methods

Study region

The Bohai Sea, is a large, turbid and shallow sea (~18 m on average – see Fig. 1) in China. The maximum depth is ~70 m at the Bohai Strait, the only channel allowing the Bohai Sea exchange with the Yellow Sea to its east. There are more than 17 rivers discharging into the Bohai Sea (see Fig. 2), of which the Huang He (Yellow River) is the largest, having an annual discharge of 420×10^8 m^3 and an annual sediment load estimated at 10^9 tons (Wei et al. 2004). The circulation pattern of the Bohai Sea is mainly dominated by the interaction of tide, density and wind driven flows (Guan 1994). The tides are mainly semi-diurnal. The speed of tidal currents ranges between 0.5-1.0 m s^{-1} in general, while the residual tidal currents are weak (Hainbucher et al. 2004). Stratification in summer and wind-driven mixing in winter are distinct, leading to high seasonality of water transparency (Shang et al. 2011). Significant hypoxia and acidification in the bottom water of the Bohai Sea have recently been observed, highlighting the stresses on this fragile ecosystem arising from human activities (Zhai et al. 2012).

For the days studied in detail here, 12 and 13th June 2011, the average wind speed over the Western Bohai Sea (120°E, 39°N) was estimated by the NOAA-NOMADS Live Access Server as 3.1 m s^{-1} and 4.3 m s^{-1} respectively, although there may be considerable spatial variability. The tidal ranges predicted by the Maritime Safety Department of the Chinese Navy for a location in Bohai Bay (118°24′48″E, 38°26′30″N) were 1.30 m and 1.61 m for the 12th and 13th June 2011 respectively. Spatial variability of tidal amplitudes in the Bohai Sea is given by (Hu and Gu 1989; Hainbucher et al. 2004). June is a month with low average discharge of the

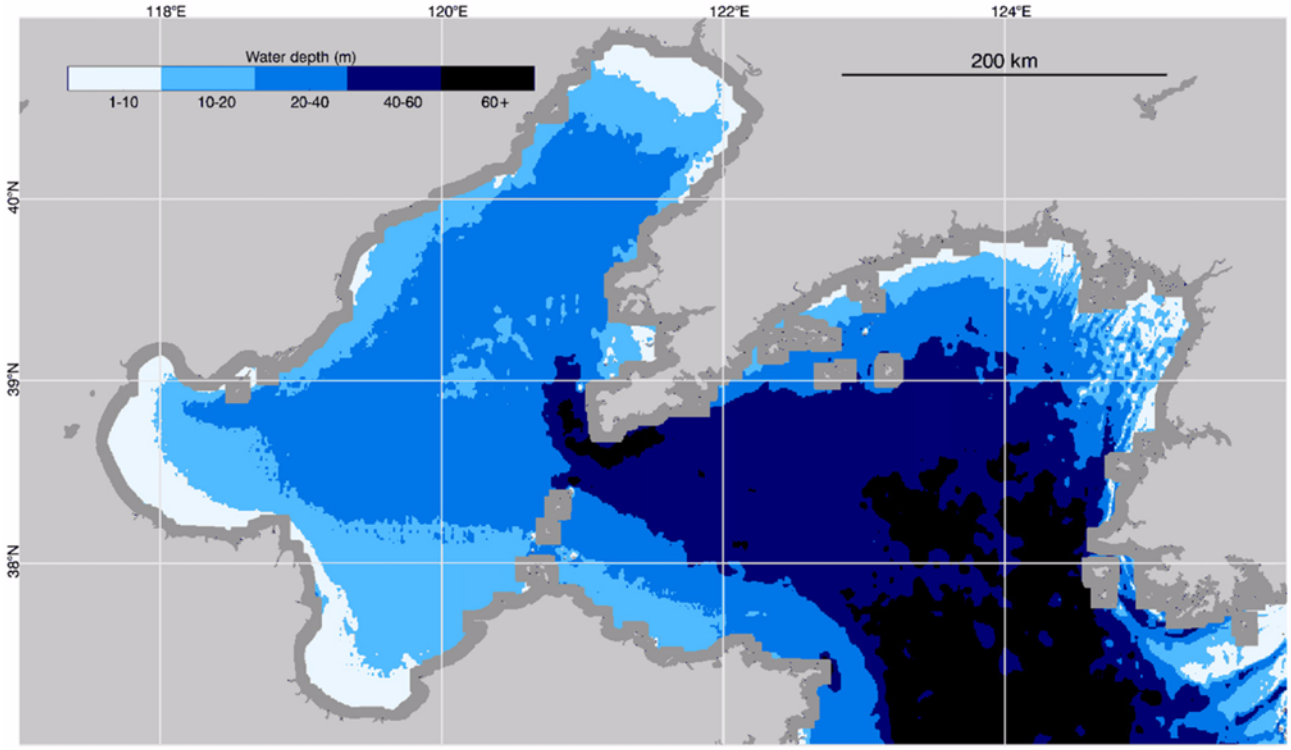

Fig. 1. Bathymetry of the Bohai Sea region using data from GEBCO_08 grid: 30' global bathymetry (http://www.gebco.net/data_and_products/gridded_bathymetry_data/). Data near the coast (within a 12.5km buffer zone) has been masked in grey here because of spurious values in the GEBCO dataset caused by lack of soundings

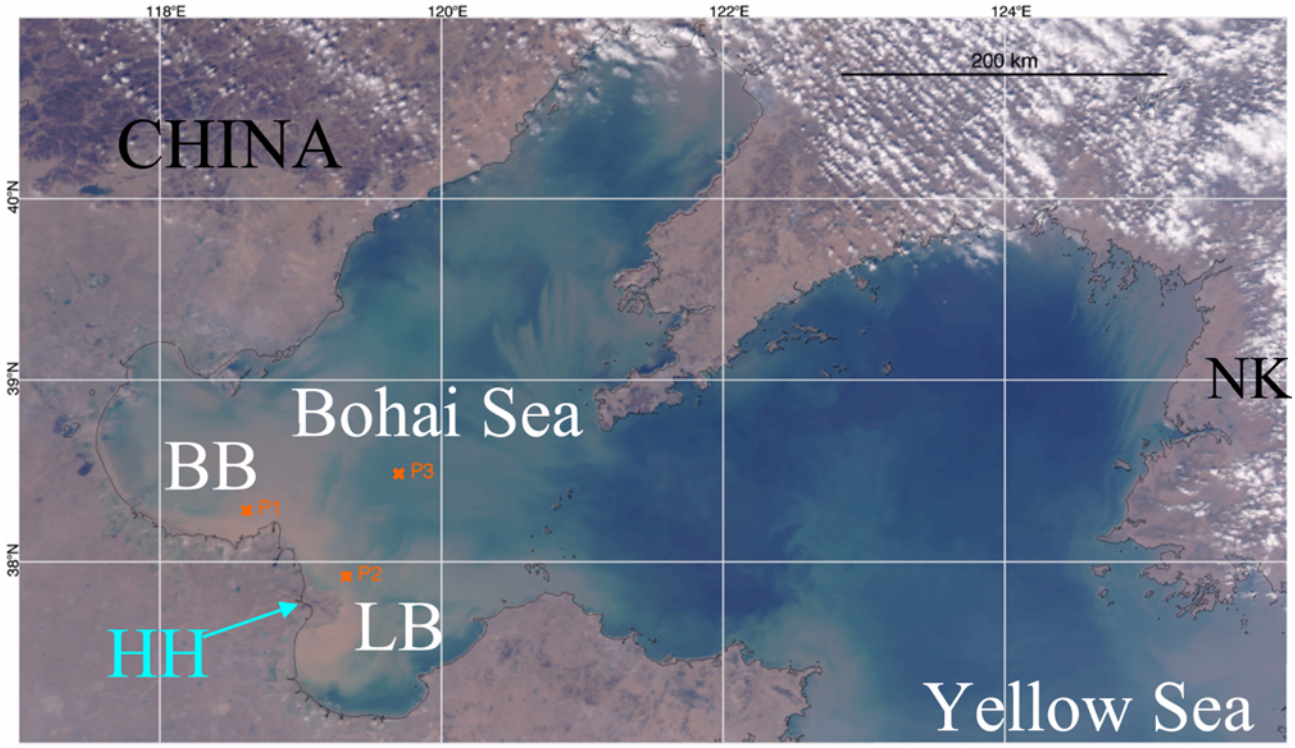

Fig. 2. Bohai Sea region showing the coastline (black line) major river discharges and using, as background, the L1 image of MODIS Aqua of 10.3.2011 (05:00) constructed as RGB image using bands 1/4/3 (645 nm/555 nm/465 nm) with custom histogram scaling. The locations P1, P2, and P3 used for study of reflectance spectra over a day are shown as red crosses with coordinates (38.282°N, 118.617°E), (37.919°N, 119.324°E) and (38.485°N, 119.696°E) respectively. NK denotes North Korea, BB and LB denote Bohai Bay and Laizhou Bay respectively, and HH denotes the Huang He (Yellow River) discharge

Yellow river, e.g. an average of 271 m^3 s^{-1} as opposed to 1481 m^3 s^{-1} in August in the data reported by (Wang et al. 2008). It is expected from previous works (Jiang et al. 2004; Wang and Li 2007; Cui et al. 2009) that SPM concentration will be low at this time of year. Some of this region is very shallow, but in general the turbidity is high enough that the bottom is not visible and therefore does not contaminate ocean colour imagery (Cui et al. 2010).

Satellite data – GOCI

GOCI Level 1B, top of atmosphere radiance, data was obtained from the Korea Ocean Satellite Center (KOSC) in November 2011 for the 12th and 13th June 2011, eight images per day. The full region was cropped to the Bohai Sea and then atmospherically corrected using the GOCI Data Processing Software (GDPS), version 1.1.0 (dated 20120629), to give level 2 (L2) data for Remote sensing reflectance, Rrs, defined as the water-leaving radiance divided by the above-water downwelling irradiance. Total Suspended Solids (TSS), and chlorophyll *a* concentration were also generated as L2 products. This georeferenced data was exported from GDPS in HDF format and imported into the ITTVIS-IDL software, where it was reprojected using a nearest neighbour interpolation onto a grid with approximately 500 m resolution over the Bohai sea (BOH grid: 37°N–41°N, 117°E–126°E). This reprojection onto a fixed grid facilitates the integration of data from multiple ocean colour sensors as described by (Vanhellemont et al. 2011) and the subsequent visualisation of multi-sensor time series (Vanhellemont and Ruddick 2011), inter-sensor product comparisons, etc.

L2 Red-Green-Blue (RGB) composites are generated from Rrs using the bands 5 (660 nm), 4 (555 nm) and 2 (443 nm), denoted hereafter Rrs660, etc. The GOCI land and "invalid" (clouds, etc.) flags are applied as a mask for all products.

The GDPS v1.1.0 atmospheric correction is based on the approach developed for SeaWiFS (Gordon and Wang 1994) but with an alternative treatment of the near infrared marine reflectance in turbid waters. A fourth order polynomial model is used to estimate Rrs745 from Rrs660

and the ratio Rrs865/Rrs745 is supposed constant. Further details on this atmospheric correction are given in (Ahn et al. 2012).

The GOCI standard "TSS" product is based on the algorithm of (Ahn et al. 2001) and is a slightly non-linear function of Rrs555 given by (Moon et al. 2010):

$$TSS = 945.07*(\mathrm{Rrs555})^{1.137} \quad (1)$$

For comparison purposes the algorithm of (Nechad et al. 2010) was applied to the GOCI 745 nm band to give a Total Suspended Matter (TSM) product:

$$TSM_{745} = A_{745}\frac{\pi*\mathrm{Rrs745}}{1-\pi*\mathrm{Rrs745}/C_{745}} \quad (2)$$

The "TSS" terminology of the GOCI product is used here for compatibility with other GOCI-related studies. This parameter, which may alternatively be termed as (the concentration of) Suspended Particulate Matter (SPM) or Total Suspended Matter (TSM), represents the dry mass concentration of particles retained after filtration of a water sample. In the present study the term SPM will be used generically, the term TSS will be specific to the GOCI TSS product and the term TSM will be specific to the product from the (Nechad et al. 2010) algorithm.

Calibration of the TSM algorithm using in situ data from the North Sea gave $A_{745} = 1755$ gm^{-3} and $C_{745} = 0.198$. While (Nechad et al. 2010) propose a complete family of algorithms for any wavelength between 520 nm and 900 nm, a product, TSM_{745}, based on the 745 nm band has been chosen in this study for two reasons. Firstly, a long wavelength with high pure water absorption ensures that high SPM concentrations can be well-estimated, avoiding the algorithm saturation (Bowers et al. 1998) expected at lower wavelengths but with the disadvantage of reduced sensitivity to low concentrations. Secondly, some results (see later) indicate that the GOCI Rrs660 and Rrs680 may be less reliable and so are avoided here.

Satellite data – MODIS-AQUA

Level 2 MODIS-AQUA images (processing version R2010.0) were downloaded from the Ocean Home Page (http://ocean.gsfc.nasa.gov/) and were also reprojected to the BOH grid. The flagging procedure is that of (Vanhellemont et al. 2011), but with the straylight flag disabled. The latter was found to be over conservative in the current study, eliminating many good data.

Validation strategy

A variety of strategies are available for the validation of ocean colour data:

- With "Matchup" analysis, satellite products for marine reflectance and water properties such as SPM concentration are compared with corresponding near-simultaneous in situ measurements. For shallow tidal seas, data with greater than 1 hour time difference is generally rejected. Dedicated seaborne validation campaigns (Moon et al. 2012) generally provide only a few matchup data points per year and so sufficient data for validation of GOCI in any specific region, such as the Bohai Sea, will probably take many more years to assemble. Continuously measuring autonomous instruments provide significantly more matchup data per year. For example, the adapted sunphotometers of the AERONET-OC network (Zibordi et al. 2009) are proving particularly efficient for validation of marine reflectance and hence the atmospheric correction algorithm. Similarly, simple, well-maintained in-water optical sensors such as single wavelength Optical Backscatter Sensors (OBS) installed on permanent moorings and backed up with (non-matchup) OBS/SPM conversion factors have proved effective for validation of satellite SPM products (Nechad et al. 2011).
- Comparisons between similar data products (Rrs or SPM) from different sensors can also provide valuable information on algorithm performance, particularly if one sensor is considered more reliable because of previous matchup validation exercises.
- Finally, even in the absence of comparison with in situ or other satellite data, a more heuristic analysis (Ruddick et al. 2002) of imagery and time series alone can indicate a variety of performance weaknesses (but not strengths!), including obviously poor flagging, negative Rrs, unphysical correlation between aerosol and marine products indicating erroneous atmospheric correction, unrealistically high/low concentrations or unrealistic correlations between products such as SPM and CHL, etc. Such analyses may be considered as unsatisfactory to users because they generally lead to negative conclusions, i.e. invalidity of products under such conditions. However, much valuable information can be obtained in this way on where algorithm improvements are needed.

In the present study, in view of the lack of sufficient data

for the region within the timespan of available GOCI data, both intersensor comparison and heuristic image analysis are adopted for satellite product validation and in situ data is used for SPM algorithm validation.

3. Results

Firstly, to put these two days of GOCI data into the perspective of longer term variability of suspended particulate matter in this region, Fig. 3 shows the time series of TSS from the algorithm given in (1), applied to the 547 nm band for location P3 during the entire MODIS-AQUA mission. This shows the importance of seasonal variability, with typical TSS concentrations of about 1-3 g m^{-3} in summer and 10-30 g m^{-3} in winter. The frequency of MODIS-TSS data for locations P1 and P2 was typically only a few pixels per year, significantly less than for P3 and insufficient to provide relevant information here.

The L2 RGB imagery for 12.6.2011 is shown in Fig. 4. This shows clearly as green patches the high turbidity areas in the Bohai Bay and Laizhuo Bay. The location of clouds varies over the seven hour time frame from first to last image. Some nearshore data in the Bohai Bay and the Laizhou Bay is also masked out here, although does not correspond to clouds. These are typically extremely turbid water areas, where the atmospheric correction algorithm can be expected to fail.

The TSS maps from the same imagery are shown in Fig. 5. In general the estimated concentrations are around 1 g m^{-3}

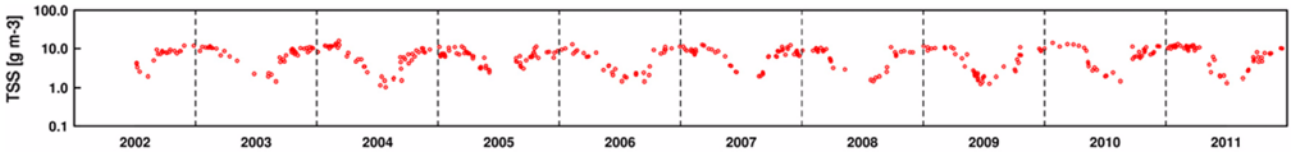

Fig. 3. Time series (2002-2011) of TSS data at location P3 from the MODIS 547 nm band

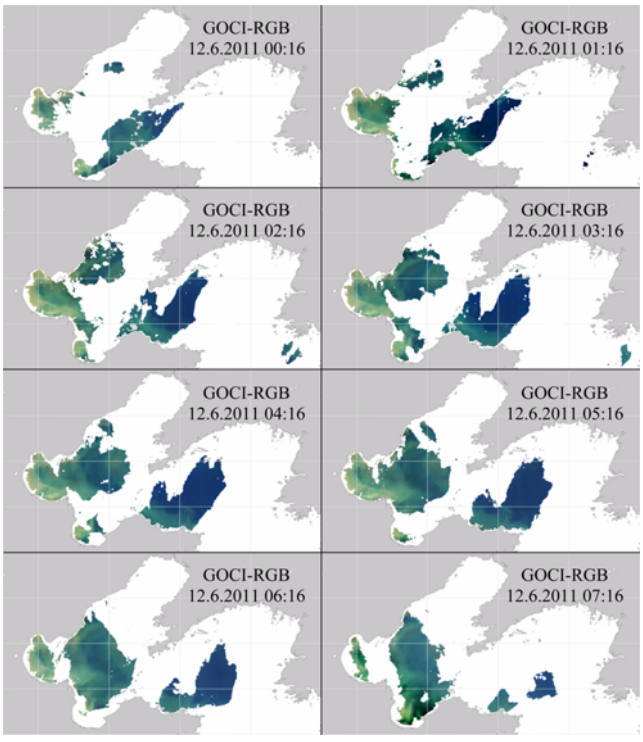

Fig. 4. L2 RGB imagery for 12.6.2011 using bands 5 (660 nm), 4 (555 nm) and 2 (443 nm) from 00:16 to 07:16 UTC, every hour. Clouds and other invalid data are shown in white; land is shown in grey

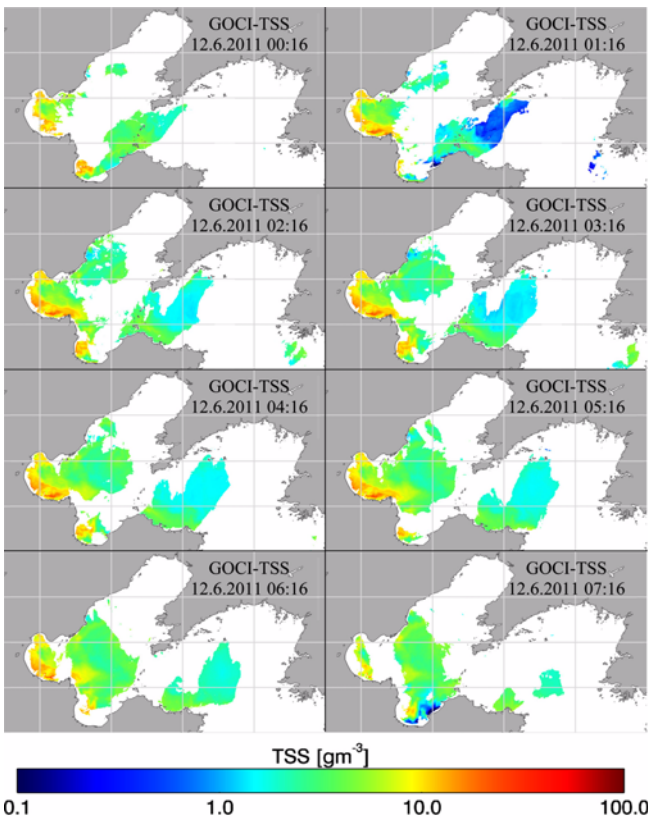

Fig. 5. TSS imagery for 12.6.2011 from 00:16 to 07:16 UTC, every hour

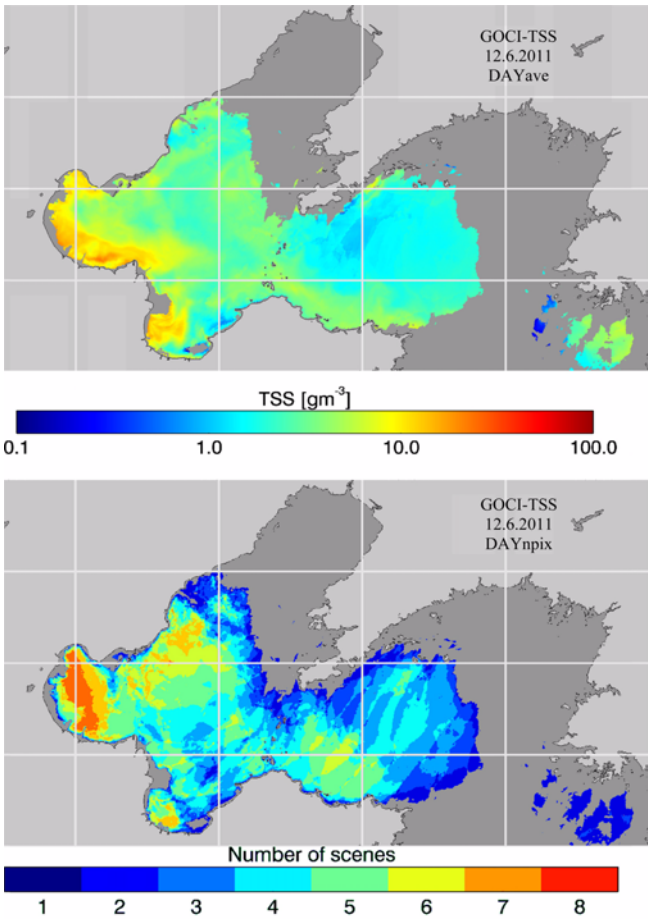

Fig. 6. Daily mean average (top) and number of valid pixels (bottom) in day for GOCI TSS data of 12.6.2011

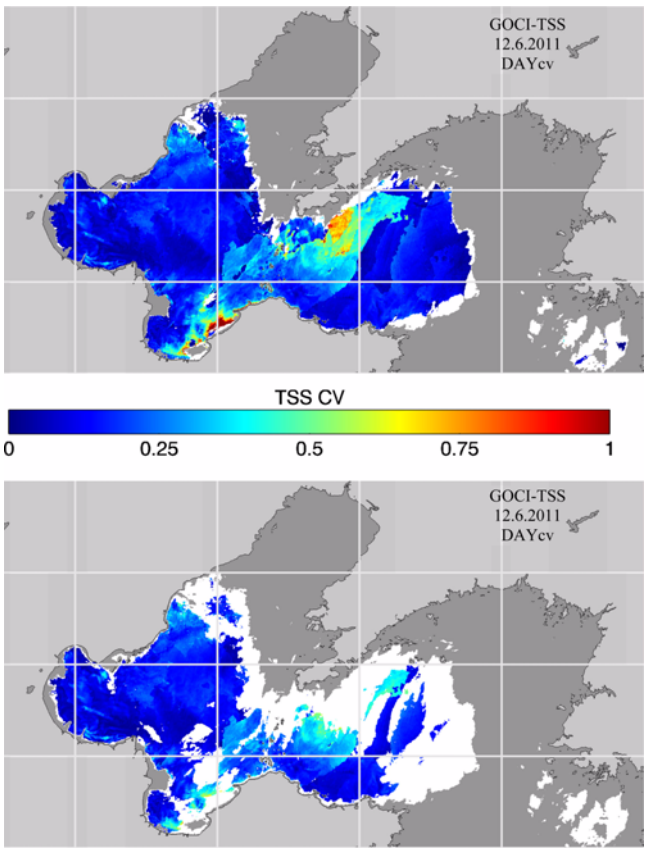

Fig. 7. Coefficient of variation (CV=Standard deviation/mean) for the daily composite shown in Fig. 6. Land is masked in light grey. For water pixels further masking is made according to the number of valid data values in the day as follows: 0 (dark grey),1 (white – top figure), 3 or less (white – bottom figure). Pixels with at least 2 (top figure) or at least 4 (bottom figure) valid data values in the day are coloured according to the colour scale from blue (low variation) to red (high variation)

in the deeper and offshore waters and range between about 1 and 40 g m^{-3} in the coastal waters of Bohai Bay and Laizhou Bay. A strong onshore-offshore gradient of depth-averaged TSS was also found in the in situ measurements of (Jiang et al. 2004), although concentrations were found to be highly variable with maxima of 8 g m^{-3} and 210 g m^{-3} recorded in the surveys of September 1998 and May 1999 respectively. The patterns of TSS match approximately the patterns found in the RGB imagery with little or no loss of data when going from RGB (Rrs) to TSS.

The daily average shown in Fig. 6 is made from the 8 instantaneous maps by mean averaging over the number of valid pixels in the day, also shown in Fig. 6. The daily average shows similar spatial patterns and numerical values to the instantaneous maps, although with a generally smoother appearance in space, as is expected from averaging of maps with small scale spatio-temporal variability. The daily average shows an obvious improvement in data availability over any individual TSS map, demonstrating the advantage of geostationary ocean colour for periods of scattered clouds.

An assessment of variability of TSS over the day is given in Fig. 7 via the Coefficient of Variation, CV (standard deviation divided by the mean in linear space). The CV maps show quite low variability, less than 25%, over most of the Bohai Sea except in regions with few images per day where one of the images (Fig. 5) has clearly erroneous data. Such regions can be identified: a) close to the coast at about (37.5°N, 120°E) where only 2 or 3 images contribute data and the last of these (see Fig. 5, 07:16 UTC) shows low values that seem to be outliers, and b) further offshore at about (38.7°, 121.6°E), again where only 2 or 3 images

contribute. These results suggest that natural variability over the day is quite low for this region on this day but that artificial variability due to processing problems can be high. High CV is effective as a means of identifying such processing problems in this case, but would be difficult to apply to more general cases with higher natural variability. In such cases, an automated outlier detection algorithm (Sirjacobs et al, 2011) based on more subtle aspects of temporal incoherency, e.g. "spikes", could be developed to harness the full extra potential of high frequency data from geostationary ocean colour.

While these TSS maps seem qualitatively plausible, with the exception of the outlier data mentioned above, their quantitative validity will depend on: a) the input Rrs data (and consequently the quality of the atmospheric correction) and b) the algorithm used to estimate TSS from Rrs. The performance of the latter algorithm is tested and compared with three additional algorithms in Appendix A, based on in situ measurements from the North Sea. The quality of the Rrs data is investigated in the following section.

Variability of Rrs over the day is depicted in Fig. 8 for three locations in Bohai Bay and Laizhou Bay. Rrs at 550 nm increases by a factor of about 3-4 going from station P3 with lowest reflectance through the intermediate station P2 to the most reflective (turbid) station P1. The water colour also changes from a blue/blue-green spectral maximum at P3 to a green spectral maximum at P1. The most surprising feature of these graphs is the apparent stability of the Rrs spectrum over the 7-hour time frame. Tidal currents are quite strong in this region (e.g. 0.5 m s^{-1}) and strong tidal variability has been previously reported by, e.g. (Jiang et al. 2004; Jiang and Wang 2005; Yu and Jian 2011) and attributed to tidal resuspension of bottom sediments.

As regards the satellite data processing, it is striking that there is greater temporal variability of Rrs at 660 nm and 680 nm than at 745 nm, although consideration of simple reflectance models (Ruddick et al. 2006) would suggest that red and near infrared reflectances should be highly correlated. An understanding of this apparent paradox would require more information on the turbid water atmospheric correction algorithm than is presently available. The relative stability over time of, for example, Rrs550 at P1 indicates both that the temporal variability of suspended particulate matter is low in this case and that the atmospheric correction is performing in a similar way for a range of air mass conditions and sun/sensor relative azimuth conditions, from morning

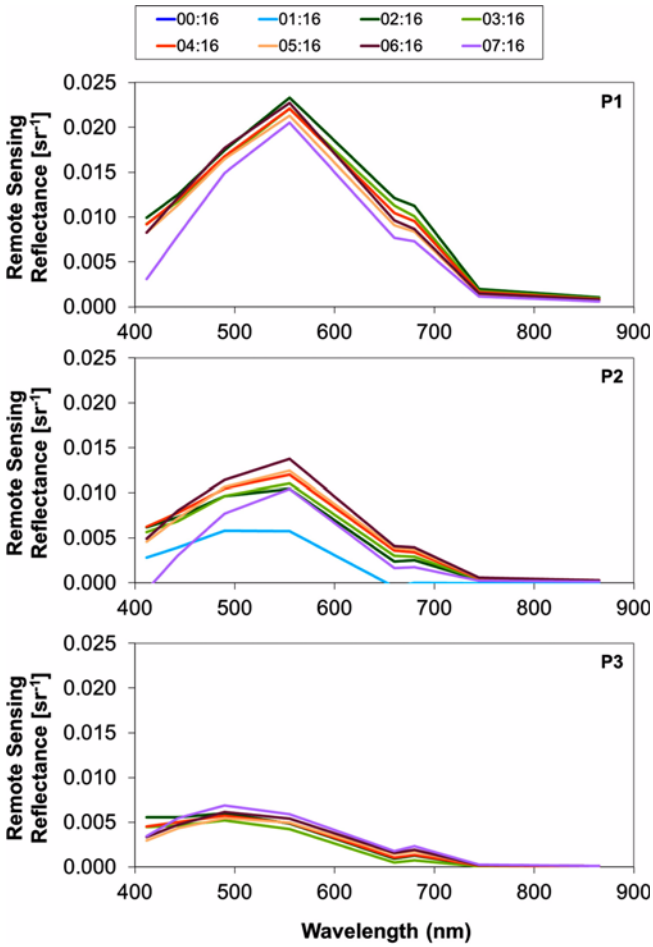

Fig. 8. Remote sensing reflectance spectra for the day 13.6.2011 recorded at 8 different hours (colour coded lines) at the three locations given in Fig. 2. Time is given in UTC. Data is unavailable (cloud/invalid masked) for 00:16 UTC at all three locations and for 01:16 UTC at P2 and P3

through noon to late afternoon. This does not exclude the possibility of systematic atmospheric correction errors, biases, but it is encouraging to note the lack of air mass dependent errors, except perhaps for the Rrs412 data at 07:16 (highest air mass) at locations P1 and P2 and the strange spectrum for 01:16 at location P2. Indeed, the most challenging conditions for an atmospheric correction algorithm will be found for the shortest wavelengths and largest air mass, where the atmospheric path reflectance from Rayleigh and aerosol scattering becomes very much greater than the marine reflectance.

These spectra show a constant ratio of Rrs745/Rrs865= 1.93, which is imposed by the turbid water atmospheric correction algorithm and is close to the value measured in situ and reported in Table 2 of (Ruddick et al. 2006) as

Rrs745/Rrs865=1.053/0.544=1.94. It has previously been shown by radiative transfer simulations, Fig. 4 of (Ruddick et al. 2006), and from satellite data (Doron et al. 2011; M Wang et al. 2012), that there will be some natural variability of Rrs745/Rrs865, particularly for the most turbid waters. The present assumption of constant Rrs745/Rrs865 has given robust performance for many previous studies based on SeaWiFS and MODIS data tracing back to (Ruddick et al. 2000) or (Hu et al. 2000), and is expected to perform well (Ruddick et al. 2006) up to Rrs780 of about 0.03, typically corresponding to SPM of about 200 g m^{-3}, but will need to be improved in future for atmospheric correction of extremely turbid waters.

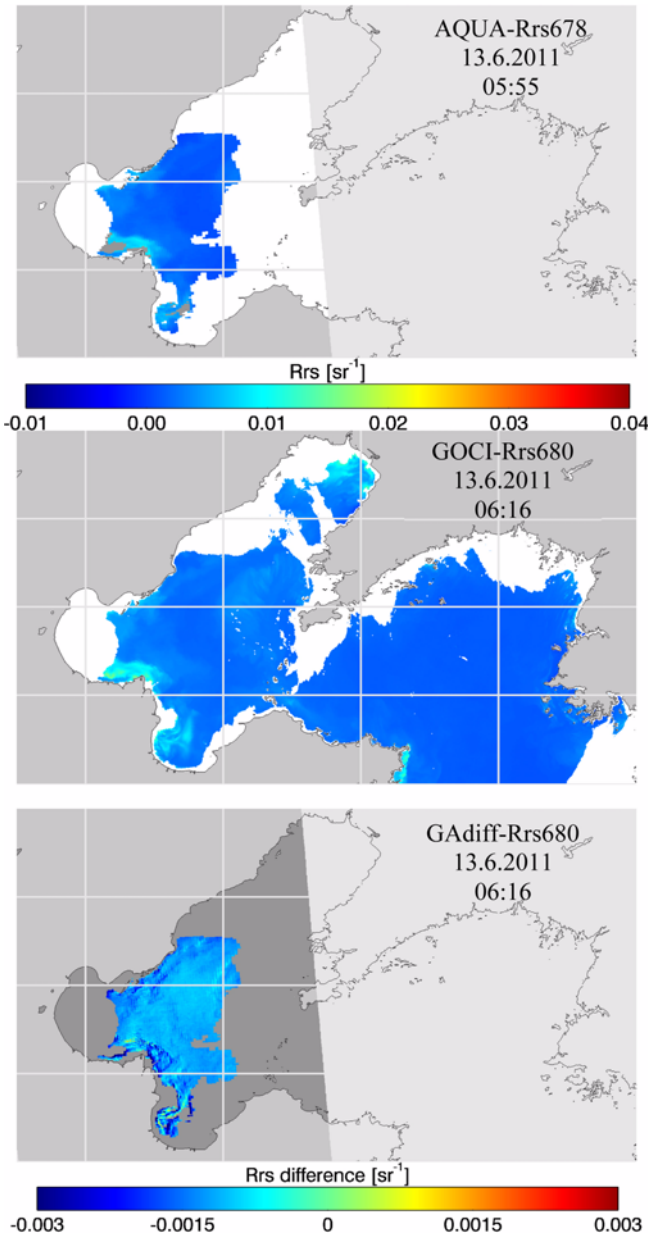

Fig. 9. Comparison of Remote sensing reflectance on 13.6.2011 for MODIS-AQUA 678nm at 05:55 UTC (top) with GOCI 680 nm at 06:16 UTC (middle) and the difference (bottom)

In Fig. 9 a comparison is shown between Rrs667 for MODIS-AQUA and the GOCI Rrs680 for a near-simultaneous image. There is an obvious difference in coverage, because the MODIS image is edge of swath and is more heavily masked for clouds. Also, one of the most turbid areas in the GOCI image (118.3°E, 38.2°N) is masked because of saturation of a MODIS band ("high_Lt" flag"). For regions where data is available from both sensors, there is a relatively constant difference of about 0.001 sr^{-1} in the clearer waters, with some larger differences, up to 0.002 or 0.003 sr^{-1} in the only turbid water region covered on that day by MODIS-AQUA.

In Fig. 10 scatterplots are shown comparing the GOCI Rrs678 with MODIS-AQUA Rrs680 for three different MODIS-AQUA images on the two days. For these three image matchups there are clear and possibly systematic differences with GOCI reflectance higher than MODIS-AQUA reflectance by about 0.001 sr^{-1} in the low reflectance waters and a regression slope varying between 0.615 and 1.06. These differences will give corresponding (nearly proportional) differences in SPM products estimated from these bands. One interesting feature of these scatterplots are the vertical stripes apparent in the scatterplot where there are multiple GOCI pixels for a single MODIS-AQUA pixel. This occurs because of the different effective spatial resolutions of the sensors, especially when MODIS data is acquired close to the edge of swath, e.g. MODIS 13.6.2012 05:55UTC.

In Fig. 11 further scatterplots are shown comparing GOCI with MODIS-AQUA for a single image matchup but now for different wavelengths, Rrs443, Rrs555 and Rrs678. Again, as found for the comparison of Rrs678, comparisons for Rrs443 and Rrs555 show typically 0.001 sr^{-1} higher reflectance for GOCI than MODIS-AQUA in the low reflectance pixels. The regression slopes are between 1.05 and 1.16, with the latter possibly affected by the difference in GOCI and MODIS-AQUA wavelengths. Further ascertaining the cause of these discrepancies is beyond the scope of this paper and would require significant extra information on the GOCI calibration and atmospheric correction. In addition to these two factors the use of a vicarious adjustment for MODIS (to match MOBY data after atmospheric correction), but not GOCI, is likely to affect any GOCI/MODIS comparison.

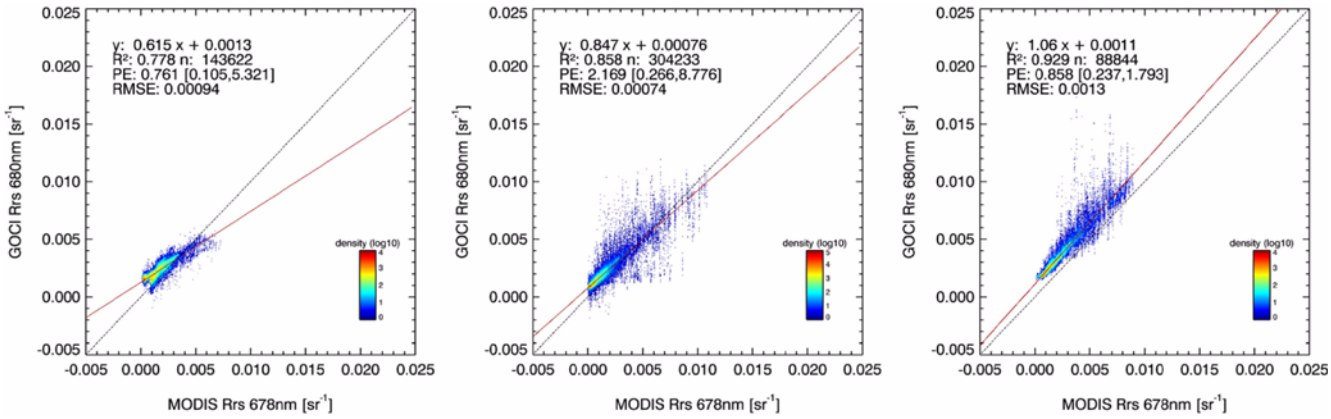

Fig. 10. Scatterplot of Remote sensing reflectance and linear correlation statistics for GOCI 680 nm and MODIS-AQUA 678 nm bands for three different MODIS/GOCI image pairs: (left) 05:10/05:16 UTC on 12.6.2011, (middle) 04:15/04:16 UTC on 13.6.2011 and (right) 05:55/06:16 UTC on 13.6.2011

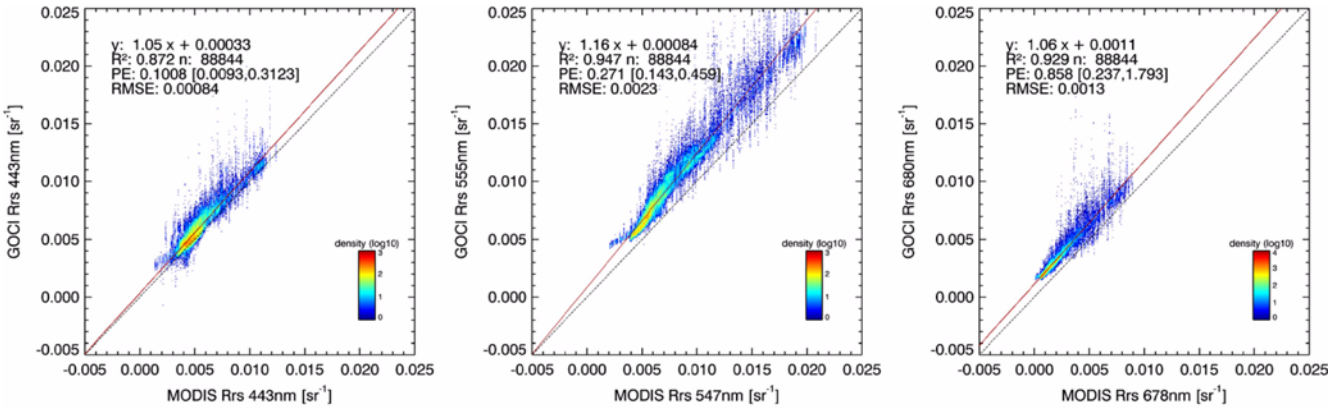

Fig. 11. Scatterplot of Remote sensing reflectance and linear correlation statistics for the GOCI/MODIS-AQUA images of 13.6.2011 06:16/05:55 UTC for three different wavelength pairs: (left) 443 nm/443 nm (middle) 555 nm/547 nm and (right) 680 nm/678 nm

4. Discussion

The potential advantages of the geostationary orbit for ocean colour observations have been well understood for a long time (Berthiaume et al. 2000). However, the technical challenges of geostationary ocean colour have also been considered as very significant. Ocean colour applications have stringent signal:noise ratio requirements and accurate atmospheric correction becomes particularly difficult at high air mass. Moreover these challenges must be met while maintaining reasonable spatial resolution and affordable mission cost. As first steps towards confronting these challenges, NASA and the European Space Agency have been developing and refining long terms plans for future geostationary ocean colour sensors (IOCCG 2012). A feasibility study has been carried out using the geostationary SEVIRI sensor for suspended matter mapping in the North Sea (Neukermans et al. 2009) and has been extended to turbidity and Photosynthetically Available Radiation (PAR) attenuation products, including extensive validation with in situ measurements (Neukermans et al. 2012b). However, the launch and successful processing of data from the GOCI sensor provides the real proof of concept, heralding a new era for ocean colour.

This paper shows first results of the Geostationary Ocean Imager (GOCI) over the turbid waters of the Bohai Sea with focus on the remote sensing reflectance and Total Suspended Solids products and including a comparison with simultaneous products from MODIS-AQUA. Total Suspended Solids maps estimated from GOCI for two days in June 2011 show concentrations typical to the lower ranges found in previous studies with in situ measurements, as expected for this time

of year from a 10-year MODIS time series. Spatial patterns of TSS are highly correlated with bathymetry, since TSS is known to be strongly related to resuspension of bottom sediments in this region.

The advantage of high frequency acquisitions from a geostationary sensor are seen clearly in the daily composite of TSS, which has a higher proportion of pixels with data than any single image, because scattered clouds traverse the region during the day. Analysis of the coefficient of variation over the day shows that natural variability of TSS was quite low (<25%) on these days in this region, but that occasional artificial variability from processing errors could be identified from the temporal variation. This result gives a first indication of the potential of improved quality control of data from geostationary ocean colour by exploitation of the natural temporal coherency of marine parameters over the day.

Some important differences were found between the GOCI standard TSS product and similar products from alternative algorithms. It is not clear at present whether these differences relate to algorithm design or algorithm calibration, e.g. for different (sub)-regions, although tests for in situ data from the North Sea show the importance of wavelength optimisation for different concentration ranges.

Remote sensing reflectance spectra for fixed points were found to show only limited variability over the day despite the expectation that natural variability at tidal time scales would be high and despite the difficult of achieving an accurate atmospheric correction at high sun zenith angle (late afternoon/early morning). Relatively greater variability over the day was found at 660 nm and 680 nm as compared to reflectances at shorter (555 nm) and longer (745 nm, 865 nm) wavelengths – this may be related to aspects of the atmospheric correction algorithm but is currently unexplained.

Comparison of MODIS and GOCI remote sensing reflectances shows a strong correlation but with an apparent offset at low reflectance (GOCI higher than MODIS-AQUA) and a slope different from one in some images. The reason for this discrepancy is not yet fully understood, although could be related to sensor calibration (including the vicarious adjustment of MODIS-AQUA, which is not performed for GOCI) and/or atmospheric correction. The higher spatial resolution of GOCI especially when MODIS-AQUA data is acquired near the edge of swath, is also notable.

Despite the good performance shown in this preliminary analysis a much more thorough analysis and validation of the GOCI imagery is required. In particular, the radiometric comparison with MODIS-AQUA and MERIS, preferably at full resolution (300 m), should be extended for other periods and the reason for the offset observed here needs to be further investigated. Performance for high air mass conditions is particularly interesting since this is thought to be a major limiting factor for geostationary ocean colour sensors. An interpretation of the causes of any radiometric differences with respect to MODIS-AQUA requires further information on the processing and extra GOCI products such as Rayleigh-corrected and aerosol reflectances from a future version of GDPS.

Both the intersensor comparison and the in situ algorithm validation raise the question of whether results for validation of a sensor or an algorithm can be extrapolated from one region to another, as supposed here. As regards turbid water atmospheric correction the "regionality" of the algorithm is contained essentially in the assumptions relating red and near infrared Rrs which are quite robust except for extremely turbid waters (Ruddick et al. 2006). Thus "region-specificity" will be related more to concentration range than to geographical location.

As regards SPM algorithms the "regionality" of an algorithm is contained primarily in the assumption of a constant ratio of mass-specific backscatter and/or absorption. The mass-specific particulate backscatter has been shown to vary between organic and inorganic particles (Neukermans et al. 2012a). Moreover, it was found that a SPM retrieval algorithm originally calibrated with data from the North Sea gave high correlation but an overestimation of SPM when applied to waters of French Guyana because of a difference in mass-specific particulate backscatter – see Fig. 5.14 of (Neukermans 2012). These differences are more directly related to particle type/origin than to geographical location and the future may lie with "regional" calibrations not, for example, for the Bohai Sea as a whole, but perhaps for temporally-varying subregions representing, say, resuspended particles, river plume particles, algal particles, etc. To make progress on this issue, a significant dataset would be required for mass-specific particulate backscatter and absorption in the many subregions of the Bohai Sea and for different seasons and even potentially for different phases of the tide in areas of resuspension. Until this is achieved we suggest that it is best to use, for this region, algorithms for turbid water atmospheric correction and SPM retrieval that have been developed at least for a similar concentration range and for predominantly inorganic particles. In this respect it is

intriguing that the SPM retrieval algorithm of (Siswanto et al. 2011), developed using data from the Yellow and East China Seas, performed rather well in tests here using in situ data from the North Sea (Appendix A).

Direct radiometric validation of GOCI with in situ data, e.g. AERONET-OC, is clearly needed. More generally, the various SPM algorithms that can be applied show quite different results and should be compared and validated on more extensive in situ data. When greater confidence has been achieved in the basic radiometric products it will be interesting to progress to more difficult-to-retrieve products, such as chlorophyll a concentration in turbid waters, and even higher level derived products such as euphotic depth or partial pressure of CO_2. The current study suggests that the GOCI data could be used now to qualitatively study sediment dynamics in the moderately turbid areas of the Bohai Sea, in combination with existing products from polar-orbiting sensors such as MODIS-AQUA and MERIS (Cui et al. 2010).

Based on the results presented in this study and those presented in the companion papers to this journal Special Issue, it is concluded that the technical challenges of geostationary ocean colour have been met by the GOCI concept. Notwithstanding potential improvements on the concept and data processing methods, it is recommended that this mission serve as a model for future geostationary ocean colour sensors over Europe/Africa and the Americas.

Acknowledgements

This study was funded by the Belgian Science Policy Office (BELSPO) STEREO programme in the framework of the GEOCOLOUR project (contract SR/00/139) and the Programme of Introducing Talents of Discipline to Universities in China (#B07034). The GRIMAS software for efficiently gridding, visualising and comparing multi-sensor and multi-temporal data (e.g. GOCI/MODIS comparisons and MODIS time series) was developed in the BELSPO funded JELLYFOR project (SR/37/135). KORDI/KOSC are thanked for supplying the GOCI data and the GDPS software and for helpful explanations regarding the GOCI algorithms and data processing. NASA is acknowledged for the MODIS-AQUA data. Bouchra Nechad is acknowledged for discussions on SPM retrieval algorithms. Two anonymous reviewers are thanked for their constructive comments on the first version of this paper.

References

Ahn JH, Park Y-J, Ryu J-H, Lee B, Oh IS (2012) Development of Atmospheric correction algorithm for Geostationary Ocean Imager (GOCI). Ocean Sci J (in this volume)

Ahn Y-H, Moon J-E, Gallegos S (2001) Development of suspended particulate matter algorithms for ocean remote sensing. Korean J Remote Sens **17**(4):285-295

Berthiaume GD, Candell LM, Hawkins JS (2000) The Special Events Imager (SEI). In: Sixth International Conference on Remote Sensing for Marine and Coastal Environments, Charlseton, South Carolina, USA, pp II-130

Bowers DG, Boudjelas S, Harker GEL (1998) The distribution of fine suspended sediments in the surface waters of the Irish Sea and its relation to tidal stirring. Int J Remote Sens **19**(14):2789-2805

Chen X, Lu J, Cui T, Jiang W, Tian L, Chen L, Zhao W (2010) Coupling remote sensing retrieval with numerical simulation for SPM study - taking Bohai Sea in China as a case. Int J Appl Earth Observ Geoinfor **12S**:S203-S211

Cui T, Zhang J, Groom S, Sun L, Smyth T, Sathyendranath S (2010) Validation of MERIS ocean- products in the Bohai Sea: A case study for turbid coastal waters. Remote Sens Environ **114**(10):2326-2336

Cui T, Zhang J, Ma Y, Zhao W-J, Sun L (2009) The study on the distribution of suspended particulate matter in the Bohai Sea by remote sensing. Acta Oceanol Sin **31**(5):10-17

Doron M, Bélanger S, Doxaran D, Babin M (2011) Spectral variations in the near-infrared ocean reflectance. Remote Sens Environ **15**:1617-1631

Faure F, Coste P, Kang G (2008) The GOCI instrument on COMS mission - The first geostationary ocean imager. In: Proceedings of the International Conference on Space Optics (ICSO), Toulouse, France, 14-17 October

Gordon HR, Wang M (1994) Retrieval of water-leaving radiance and aerosol optical thickness over the oceans with SeaWiFS: A preliminary algorithm. Appl Optics **33**(3):443-452

Guan B (1994) Patterns and structures of the currents in Bohai, Huanghai and East China Sea. In: Zhou D, Liang Y, Tseng C (eds) Oceanology of China Sea. Kluwer Academic Publishers, pp 17-26

Hainbucher D, Hao W, Pohlmann T, Feng S, Suendermann J (2004) Variability of the Bohai Sea circulation based on model calculations. J Mar Syst **44**(3):153-174

Hu C, Carder KL, Muller-Karger F (2000) Atmospheric correction of SeaWiFS imagery over turbid coastal waters: A practical method. Remote Sens Environ **74**:195-206

Hu F,Gu G (1989) Seasonal changes of the mean tidal range along the Chinese coasts. Oceanol Limnol Sin **20**(5):401-411

IOCCG (2012) Ocean Colour observations from a geostationary orbit. In: Antoine D (ed) IOCCG/SCOR report 12, pp 102

Jiang W, Pohlmann T, Sun J, Starke A (2004) SPM transport in the Bohai Sea: field experiments and numerical modelling. J Mar Syst **44**:175-188

Jiang WS, Wang HJ (2005) Distribution of suspended matter and its relationship with sediment particle size in Laizhou bay. Oceanol Limnol Sin **36**(2):97-103

Mazeran C, Meskini N (2008) Mission Couleur de l'Océan Géostationnaire: Charactérisation de la géométrie, gain en couverture, impact d'instabilites instrumentals CNES-0440R650-RF-v1

Moon J-E, Ahn Y-H, Ryu J-H, Shanmugam P (2010) Development of ocean environmental algorithms for Geostationary Ocean Color imager (GOCI). Korean J Remote Sens **26**(2):189-207

Moon J-E, Park YJ, Ryu J-H, Choi J-K, Ahn J-H, Min J-E, Son Y-B, Lee S-J, Han H-J, Ahn Y-H (2012) Initial validation of GOCI water products against in situ data collected around Korean peninsula for 2010-2011. Ocean Sci J (in this volume)

Nechad B, Alvera-Azcaràte A, Ruddick K, Greenwood N (2011) Reconstruction of MODIS Total Suspended Matter time series maps by DINEOF and validation with autonomous platform data. Ocean Dyn **61**:1205-1214

Nechad B, Ruddick KG, Park Y (2010) Calibration and validation of a generic multisensor algorithm for mapping of Total Suspended Matter in turbid waters. Remote Sens Environ **114**:854-866

Neukermans G (2012) Optical in-situ and geostationary satellite-borne observations of suspended particles in coastal waters. Ph.D. Thesis, Université du Littoral Côte d'Opal, Academic and Scientific Publishers, Brussels, Belgium

Neukermans G, Loisel H, Mériaux X, Astoreca R, McKee D (2012a) In situ variability of mass specific beam attenuation and backscattering of marine particles with respect to particle size, density and composition. Limnol Oceanogr **75**(1):124-144

Neukermans G, Ruddick K, Bernard E, Ramon D, Nechad B, Deschamps P-Y (2009) Mapping total suspended matter from geostationary satellites: A feasibility study with SEVIRI in the Southern North Sea. Opt Express **17**(16):14029-14052

Neukermans G, Ruddick K, Greenwood N (2012b) Diurnal variability and light attenuation in the southern North Sea from the SEVIRI geostationary sensor. Remote Sens Environ **124**:564-580

Ruddick K, De Cauwer V, Park Y, Becu G, De Blauwe J-P, Vreker ED, Deschamps P-Y, Knockaert M, Nechad B, Pollentier A, Roose P, Saudemont D, v Tuyckom D (2002) Preliminary validation of MERIS water products for Belgian coastal waters. In: Envisat Validation workshop, European Space Agency, Frascati, 9-13 December

Ruddick KG, De Cauwer V, Park Y, Moore G (2006) Seaborne measurements of near infrared water-leaving reflectance - the similarity spectrum for turbid waters. Limnol Oceanogr **51**(2):1167-1179

Ruddick KG, Ovidio F, Rijkeboer M (2000) Atmospheric correction of SeaWiFS imagery for turbid coastal and inland waters. Appl Optics **39**(6):897-912

Schmetz J, Pili P, Tjemkes S, Just D, Kerkmann J, Rota S, Ratier A (2002) An introduction to METEOSAT Second Generation (MSG). Bull Am Meteorol Soc **83**(7):977-992

Shang SL, Lee ZP, Wei GM (2011) Characterization of MODIS-derived Euphotic Zone Depth: Results for the China Sea. Remote Sens Environ **115**(1):180-186

Shen F, Verhoef W, Zhou Y, Salama MS, Liu X (2010) Satellite estimates of wide-range suspended sediment concentrations in Changjiang (Yangtze) estuary using MERIS data. Estuar Coast **33**:1420-1429

Sirjacobs D, Alvera-Azcárate A, Barth A, Lacroix G, Park Y, Nechad B, Ruddick K, Beckers J-M (2011) Cloud filling of ocean and sea surface temperature remote sensing products over the Southern North Sea by the Data Interpolating Empirical Orthogonal Functions methodology. J Sea Res **65**:114-130

Siswanto E, Tang J, Yamaguchi H, Ahn Y-H, Ishizaka J, Yoo S, Kim S-W, Kiyomoto Y, Yamada K, Chiang C, Kawamura H (2011) Empirical ocean-colour algorithms to retrieve chlorophyll-a, total suspended matter, and dissolved organic matter absorption coefficient in the Yellow and East China Seas. J Oceanogr **67**:627-650

Vanhellemont Q, Nechad B, Ruddick K (2011) GRIMAS: Gridding and archiving of satellite-derved ocean colour data for any region on earth. In: COASTGIS conference, Oostende

Vanhellemont Q, Ruddick K (2011) Generalized satellite image processing: Eight years of ocean colour data for any region on earth. In: Proceedings of the SPIE Remote Sensing conference, Prague

Wang F, Li G-s (2007) Two parameters retrieval models of suspended sediment concentration of Bohai Sea based on MODIS data. Geogr Res **26**(6):1186-1196

Wang L, Zhao D, Yang J, Chen Y (2012) Retrieval of total suspended matter from MODIS 250m imagery in the Bohai Sea of China. J Oceanogr. doi: 10.1007/s10872-012-0129-5

Wang M, Shi W, Jiang L (2012) Atmospheric correction using near-infrared bands for satellite ocean data processing in the turbid western Pacific region. Opt Express **20**(2):741-753

Wang Q, Guo X, Takeoka H (2008) Seasonal variations of the Yellow River plume in the Bohai Sea: A model study. J Geophys Res **113**:C08046. doi: 10.1029/2007JC004555

Wei H, Sun J, Moll A, Zhao L (2004) Phytoplankton dynamics in the Bohai Sea-observations and modelling. J Mar Syst **44**(3):233-251

Yu LL, Jian WS (2011) Seasonal variations in the distributions of suspended fine particulate matter in the Yellow Sea and the East China Sea. Oceanol Limnol Sin **42**(4):474-481

Zhai W, Zhao H, Zheng N, Xu Y (2012) Coastal acidification in summer bottom oxygen-depleted waters in northwestern-northern Bohai Sea from June to August in 2011. Chinese Sci Bull **57**(9):1062-1068

Zhang J (1996). Nutrient elements in large Chinese estuaries. Cont Shelf Res **16**(8):1023-1045

Zibordi G, Holben B, Slutsker I, Giles D, D'Alimonte D, Mélin F, Berthon J-F, Vandemark D, Feng H, Schuster G, Fabbri EE, Kaitala S, Seppälä J (2009) AERONET-OC: A network for the validation of ocean primary product. J Atmos Ocean Tech **26**:1634-1651

Appendix A. A comparison of SPM algorithms using data from the North Sea

In this Appendix the GOCI standard TSS algorithm (1), denoted TSS_{GOCI} and the MUMM 745 nm band TSM algorithm (2), denoted TSM_{745}, are compared using in situ data from the North Sea with three additional algorithms not considered in the main text. Two of these algorithms are constructed using the same theoretical basis and calibration (Nechad et al. 2010) as TSM_{745}, but using instead the wavelengths 555 nm and 660 nm respectively:

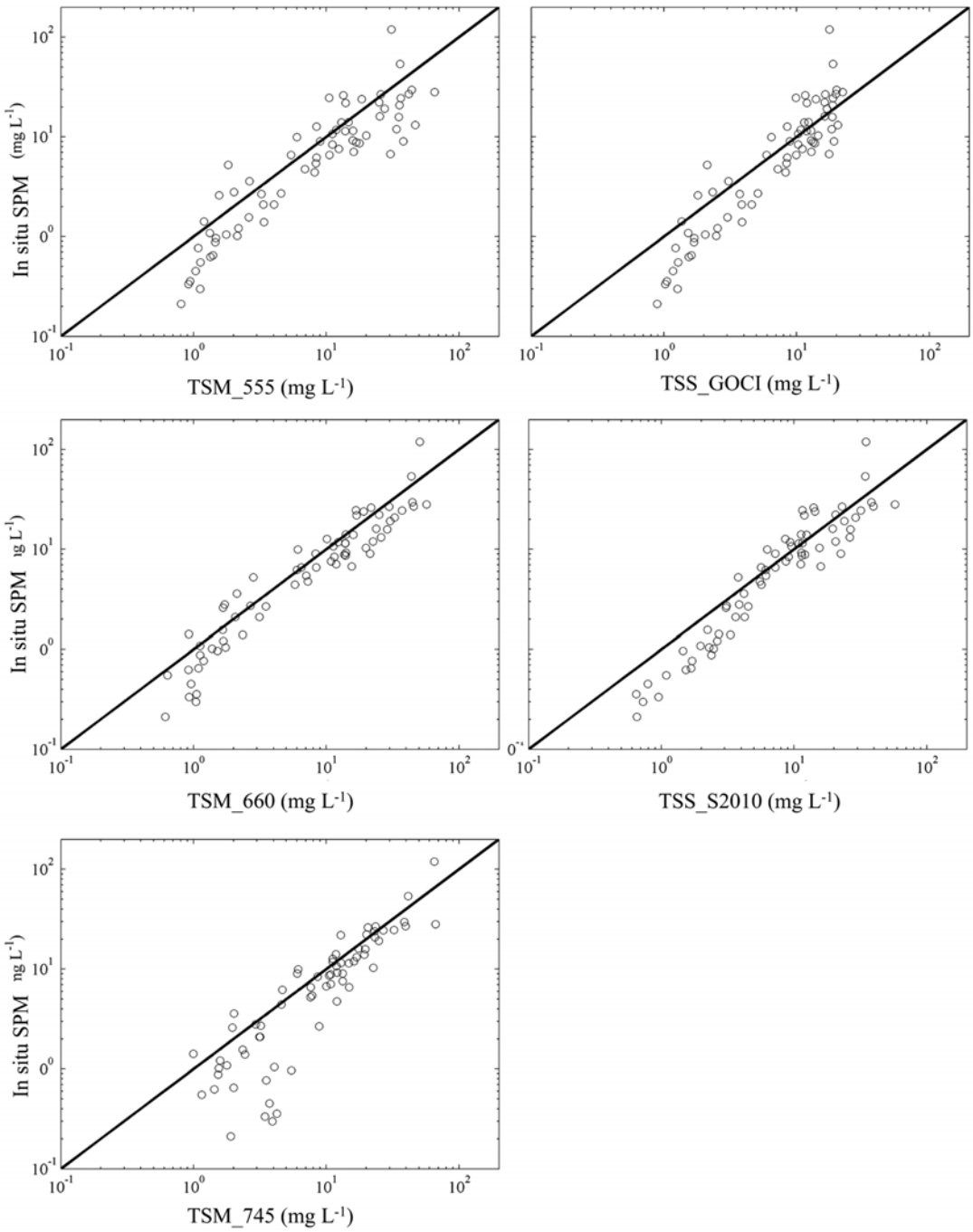

Fig. A1. Scatter plots of in situ SPM against estimates from the remote sensing algorithms of Nechad et al (2010) applied to the 555 nm (top-left), 660 nm (middle-left) and 745 nm (bottom-left) bands as well as the GOCI standard 555 nm (top-right), and Siswanto et al. (2011, middle-right) algorithms for data collected in the southern North Sea. The black line represents the 1:1 line

Table A1. Percentiles of prediction error and log-log regression slope, offset and correlation coefficient (r) for the Suspended Particulate Matter algorithms tested with North Sea data in Appendix A. Best performance corresponds to lowest PE for each percentile

	Percentiles of PE			log-log regression		
	P5	P50	P95	Slope	Offset	r
TSS_GOCI (555 nm)	4%	50%	196%	1.320	-0.343	0.928
TSS_S2011	7%	41%	159%	1.207	-0.286	0.953
TSM_555	4%	58%	274%	1.026	-0.170	0.915
TSM_660	2%	40%	179%	1.028	-0.127	0.954
TSM_745	5%	38%	814%	1.196	-0.361	0.877

$$TSM_{555} = A_{555}\frac{\pi * Rrs555}{1-\pi * Rrs555/C_{555}} \quad (3)$$

$$TSM_{660} = A_{660}\frac{\pi * Rrs660}{1-\pi * Rrs660/C_{660}} \quad (4)$$

where $A_{555} = 111.8\ gm^{-3}$ and $C_{555} = 0.145$ and $A_{660} = 327.8\ gm^{-3}$ and $C_{660} = 0.171$.

The third additional algorithm, TSS_{S2011} is that of (Siswanto et al. 2011), and was developed using Yellow and East China Sea data:

$$\log_{10}TSS_{S2011} = 0.738+22.79*(Rrs555+Rrs670) - 0.574*\frac{Rrs490}{Rrs555} \quad (5)$$

Simultaneous in-situ measurements of SPM and marine reflectance collected in the southern North Sea between 2007 and 2010 were used. Remote sensing reflectance is derived from hyperspectral above-water radiance and irradiance measurements recorded with a set of TriOS Ramses radiometers as described in (Ruddick et al. 2006) and its web appendices. Spectral integration is made using the MODIS-AQUA spectral response functions. Details of the measurement protocol for SPM and data selection criteria can be found in (Neukermans 2012).

Fig. A1 illustrates the performance of these remote sensing algorithms for prediction of SPM in the southern North Sea. The 5th, 50th, and 95th percentile values of the prediction error: PE=100%*|SPM(in situ)-SPM(RS)|/SPM(in situ) are given in Table A1.

Reasonable performance is seen for all five algorithms with median (P50) prediction errors ranging between 38% and 58% and log-log correlation coefficient ranging between 0.877 and 0.954. Most noticeable in the scatterplots is the poor performance of the TSM_745 algorithm for low SPM, where relative errors on the reflectance may be most important, and, for high SPM, the increased scatter (TSM_555) or threshold (TSS_GOCI) for the algorithms based on the 555 nm band. A similar consideration of the compromise between SPM algorithm saturation at high reflectance and the difficulty of accurately measuring reflectance at low reflectance led (Shen et al. 2010) to propose a switching algorithm, using increasing wavelength (increasing pure water absorption) for retrieval of higher SPM concentrations.